

DEVELOPMENT OF STRESS-STRAIN RELATION AND FAILURE ASSESSMENT METHOD FOR PREDICTING INITIATION OF DUCTILE FRACTURE IN VARIOUS ALLOYS

Yukio Takahashi¹, Haruhisa Shegeyama²

¹ Research Advisor Emeritus, Central Research Institute of Electric Power Industry, Kanagawa, Japan (yukio@criepi.denken.or.jp)

² Principal Researcher, Central Research Institute of Electric Power Industry, Kanagawa, Japan

ABSTRACT

In evaluating the margin against fracture or loss of function under various loading including some hypothetical one, resistance against initiation and propagation of ductile fracture needs to be evaluated. As for the initiation of ductile fracture from the originally defect-free structures, plastic strain plays a crucial role as a driving force for micromechanical damage such as void formation and growth but stress multiaxiality also has some subsidiary effect through the involvement in such a process. Prediction of plastic strain and stress state in structures needs stress-strain relations to be implemented in finite element analysis. In order to avoid the necessity of testing the material and processing the data each time, true stress-strain relations whose constants can be determined from fundamental properties such as proof stress, tensile strength, rupture elongation and reduction of area were developed based on the results of tensile tests on various alloys used in nuclear power plants in this study. Tensile tests were also conducted for notched round bar and grooved plate specimens made from four representative materials used in nuclear power plants. As a result of the analyses using the developed stress-strain relations, effect of damage on deformation behavior as well as failure strain were identified. Then the dependency of failure strain and damage rate on stress triaxiality factor and the third invariant of deviatoric stress tensor was determined through the repeated damage-coupled analyses and comparisons of load-displacement curves. Although constants needed to be adjusted according to materials and temperatures, reasonable agreement between predicted load-displacement curves and test records was achieved for all the materials and test specimens investigated, indicating the effectiveness of the present approach.

INTRODUCTION

In order to evaluate the structural integrity of various components and structures, methods for estimating the material/structural behaviour under various loading conditions are indispensable. It is widely recognized that the combination of elastic-plastic analysis and strain-based failure criteria are more effective than the procedure based on the stress calculated elastically in evaluating the initiation of fracture at the portion with concentrated inelastic strain. This is one of the situations expected to take place when some of the components in nuclear power plants experience severe loading in design basis or beyond design basis events. Several codes published by Japan Society of Mechanical Engineers (2014, 2015ab, 2018) addressed the need of such evaluation for reactor containment vessels by employing stress-strain equations and failure criteria recommended in Section VIII in Boiler and Pressure Vessel Codes in American Society of Mechanical Engineers (2017). However, there are not sufficient evidence about their applicability to various structural materials used in nuclear power plants.

Under such circumstance, the authors have been working for the purpose of developing the reliable tools for evaluating ultimate strength using nonlinear finite element (FE) analysis for several years. As a part of this activity, equations for describing true stress-true strain relations were developed for various alloys used in nuclear power plants, including ferritic and austenitic steels as well as one of Nickel based alloys. Capability for describing the deformation behavior before and after the necking formation in plain bar specimens was studied through a series of tensile tests and accompanying FE analyses. Equations describing the true stress-true strain relation have been developed and their

applicability to various materials used in nuclear power plants has been shown (Takahashi, 2018, 2021, 2023). Additional tensile tests have also been performed for circumferentially notched bar and grooved flat plate specimens for four materials in order to cover a wide range of the stress multiaxiality to develop methods for simulating their behavior by FE analysis in consideration of the effects of stress multiaxiality on failure as well as deformation. Outline of the outcome obtained through these efforts is summarized here.

EQUATIONS REPRESENTING TRUE STRESS-TRUE STRAIN RELATIONS

Objective

In order to perform reliable assessment using elastic-plastic analysis for any structure using FE method, it is critically important to adopt an appropriate constitutive model which can express the deformation behavior of the targeted material with a sufficient accuracy. In the case of analysis for monotonically increasing loading without a large deviation from proportional loading or some cyclic loading without reversed plastic deformation, equations describing the relation between equivalent stress and equivalent plastic strain principally governs the accuracy of prediction within the framework of isotropic hardening rule. As the plastic strain at failure often called ductility is generally large in most metallic materials, relation between true stress and true plastic strain is necessary to apply, rather than nominal (engineering) stress-nominal strain relations obtained in uniaxial tensile tests. Construction of the true stress-strain curves from fundamental information has been sought and the following formulations have been obtained.

Type I formulation

So-called Swift's equation written as

$$\varepsilon_p + \bar{\varepsilon}_p = (\sigma / \sigma_0)^n \quad (1)$$

was employed as a starting point of the development of the model. Here ε_p and σ are true plastic strain and true stress whereas $\bar{\varepsilon}_p$, σ_0 and n are three constants to be changed with material and temperature. By assuming that stress at a certain amount of plastic strain, say 0.002, ε_y , is known as the yield stress, σ_y , and true stress and true plastic strain at the maximum load are known as $\sigma_{u,t}$ and ε_u eq. (1) can be rewritten as

$$\sigma = \left\{ \frac{(\varepsilon_p - \varepsilon_y)\sigma_{u,t}^n + (\varepsilon_u - \varepsilon_p)\sigma_y^n}{\varepsilon_u - \varepsilon_y} \right\}^{1/n} \quad (2)$$

Here $\sigma_{u,t}$ and ε_u can be calculated simply by

$$\begin{aligned} \sigma_{u,t} &= (1 + e_u)\sigma_u \\ \varepsilon_u &= \ln(1 + e_u) - \sigma_{u,t} / E \end{aligned} \quad (3)$$

from the ultimate tensile strength, σ_u and corresponding nominal strain often called uniform elongation, e_u and Young's modulus, E .

It was found that this equation can describe the deformation behavior of many materials reasonably well up to the point of maximum load but quite often fails to predict the strain at maximum load and the subsequent decrease of nominal stress accompanying progress of necking. Therefore another equation which ensures the attainment of maximum load at uniform elongation was added to cover the whole deformation range as

$$\sigma = \left\{ \frac{(\varepsilon_p - \varepsilon_y)\sigma_{u,t}^n + (\varepsilon_u - \varepsilon_p)\sigma_y^n}{\varepsilon_u - \varepsilon_y} \right\}^{1/n} \quad \text{for } \varepsilon_p \leq 0.95\varepsilon_u \quad (4)$$

$$= \sigma_{0.95\varepsilon_u} (\varepsilon_p / 0.95\varepsilon_u)^{\varepsilon_u} \quad \text{for } \varepsilon_p > 0.95\varepsilon_u$$

with an aid of the following parameter representing the true stress at $0.95\varepsilon_u$ predicted by equation (2) as:

$$\sigma_{0.95\varepsilon_u} = \left\{ \frac{(0.95\varepsilon_u - \varepsilon_y)\sigma_{u,t}^n + 0.05\varepsilon_u\sigma_y^n}{\varepsilon_u - \varepsilon_y} \right\}^{1/n} \quad (5)$$

In this formulation, uniform elongation, e_u and the hardening exponent, n , play critical roles to determine the form of stress-strain curve. In order to determine these parameters from the information readily available, the following equations were developed based on regression analyses for test data on various materials as shown in a previous paper (Takahashi, 2023), excluding the coefficient, 1.1, in eq. (6) which was added in order to make a correction for the constraint given by the ridge machined for installing an extensometer.

$$e_u = 1.1(0.0095\varepsilon_f - 0.0016\delta) \quad (6)$$

$$n = 7.26 - 2590(\sigma_u - \sigma_y) / E - 2.08e_u \quad (7)$$

where ε_f and δ are rupture elongation and reduction of area both represented in mm/mm. A total set of these equations enables one to construct true stress – true plastic strain relation from the fundamental information normally reported as a result of tensile tests, i.e. 0.2% proof stress, tensile strength, rupture elongation and reduction of area.

Type II formulation

Based on a later finding of relatively poor accuracy of the Swift equation in some of the ferritic steel due to difficulty of approximating true stress -true plastic strain curve up to maximum load by one power law relation, the alternative set of equations was developed for the application to various ferritic steels having a wide variety of strength and ductility. In this model, total stress-strain curve is divided into three regions and different equations are used for each region.

The first region is expressed by the equation similar to the one used on type I formulation as

$$\sigma = \left\{ \frac{(\varepsilon'_p - \varepsilon_y)\sigma_{u,t}^n + (\varepsilon'_u - \varepsilon'_p)\sigma_y^n}{\varepsilon'_u - \varepsilon_y} \right\}^{1/n} \quad (8)$$

but the yield plateau up to the yield strain, ε_y , is described by substituting the following value instead of plastic strain, ε_p .

$$\varepsilon'_p = \max(\varepsilon_p, \varepsilon_y) \quad (9)$$

Another modification is an employment of corrected value for uniform elongation denoted as ε'_u , which is generally smaller than the actual uniform elongation, ε_u , itself.

The second and third regions are more simply expressed by

$$\sigma = \sigma_{u,t} - K \left\{ \frac{\varepsilon_u - \varepsilon_p}{\varepsilon_u} \right\}^2 \quad (10)$$

and

$$\sigma = \sigma_{u,t} \left(\varepsilon_p / \varepsilon_u \right)^{\varepsilon_u} \quad (11)$$

respectively, using the true stress, $\sigma_{u,t}$, and true plastic strain, ε_u , at maximum load obtained by eq. (3). With the relationship between the stresses calculated by these equations in consideration, the whole relation can be summarized as

$$\sigma = \min \left[\left\{ \frac{(\varepsilon'_p - \varepsilon_y) \sigma_{u,t}^n + (\varepsilon'_u - \varepsilon'_p) \sigma_y^n}{\varepsilon'_u - \varepsilon_y} \right\}^{1/n}, \sigma_{u,t} - K \left\{ \frac{\varepsilon_u - \varepsilon_p}{\varepsilon_u} \right\}^2, \sigma_{u,t} \left(\varepsilon_p / \varepsilon_u \right)^{\varepsilon_u} \right] \quad \text{for } \varepsilon_p \leq \varepsilon_u \quad (12)$$

$$= \sigma_{u,t} \left(\varepsilon_p / \varepsilon_u \right)^{\varepsilon_u} \quad \text{for } \varepsilon_p > \varepsilon_u$$

This set of equations includes several parameters to be determined. At first, ε_y was modeled by a function of absolute temperature, T_{abs} commonly as

$$\varepsilon_y = \max \{ 0.002, 0.06181 / \exp(0.005455 T_{abs}) \} \quad (13)$$

based on the test data on various ferritic steels. Then the behavior in the first region is described by changing the values of n and ε'_u according to the following equations:

$$n = 6.545 / (\sigma_u / \sigma_y)^{1.0163} \quad (14)$$

$$\varepsilon'_u = 0.2723 n^{0.6875} \varepsilon_u \quad (15)$$

The second region is characterized by K calculated by

$$K = 51.03 (\sigma_u - \sigma_y)^{0.2653} \quad (16)$$

It should be noted that one can construct true stress-true plastic strain relation only from the information readily available, as in the type I formulation, in spite of more complicated appearance.

EQUATIONS REPRESENTING DUCTILE FAILURE CRITERIA AND DAMAGE EFFECT

Objective

It is well known that micro-voids form and grow with plastic deformation and constitutes the main mechanism of ductile fracture of ductile metallic materials. As the presence of such voids affects macroscopic deformation behavior also, inclusion of its effect into constitutive relation might be important for accurate estimation of ductile fracture behavior. In particular, its consideration becomes more important as the stress triaxiality increases and development of voids is accelerated in comparison with uniaxial stress condition. Although more complicated model such as so-called GTN model incorporating the equations describing initiation, growth and coalescence of micro-voids separately was proposed (Gurson, 1967, Tvergaard and Needleman, 1984) and has been applied to various materials for a long time, a simpler approach was selected in the present study in order to make the application easier, considering the requirement of large effort for identification of material constants. Outline of the approach developed here will be given in what follows.

Evaluation of local failure

In our approach, it is assumed that local failure occurs when the damage valuable demoted by D reaches one as

$$D = 1 \quad (17)$$

It is also assumed that its rate is given by

$$\dot{D} = \overline{\dot{\varepsilon}}_p / \varepsilon_f \quad (18)$$

using equivalent plastic strain rate, $\overline{\dot{\varepsilon}}_p$ and true rupture ductility, ε_f as in the approach taken by Oh et al. (2010), ε_f plays a crucial role of determining the failure characteristics and the following expression is employed in this study.

$$\varepsilon_f = (1 - \omega)\varepsilon_{f0} / \exp(\alpha h) + \omega\varepsilon_{\omega 0} / \exp(\beta h) \quad (19)$$

where h and ω are two parameters characterizing multiaxial stress state by being defined by

$$\varepsilon_f = (1 - \omega)\varepsilon_{f0} / \exp(\alpha h) + \omega\varepsilon_{\omega 0} / \exp(\beta h) \quad h = 3\sigma_m / \bar{\sigma} \quad (20)$$

$$\omega = 1 - \frac{27 J_3^2}{2 \bar{\sigma}^2} \quad (21)$$

using mean stress, σ_m , von Mises equivalent stress, $\bar{\sigma}$ and the third invariant of the deviatoric stress tensor, J_3 . Other variables in eq. (18) are material- and temperature-dependent constants expressing the different characteristics in terms of the influences of stress states. Dependency on stress triaxiality is based on the functional form derived by Rice and Tracey (1969). On the other hand, inclusion of the effect of the third invariant of the deviatoric stress tensor has been proposed in many recent studies (e.g. Bonora and Testa, 2022) and it was followed here based on the finding of the difficulty of modeling the failure behavior of the four types of specimens with the effect of stress triaxial factor alone.

Consideration of the effect on deformation behavior

In some materials dealt with in this study, deformation behavior before failure seemed to be influenced by damage as well as the value of ω . Therefore these effects are taken into account by making flow stress change according to

$$\bar{\sigma} = (H' - \chi\omega)\overline{\dot{\varepsilon}}_p - \gamma \left\{ \dot{D} - \overline{\dot{\varepsilon}}_p / \varepsilon_{f0} \exp(-\alpha) \right\} \bar{\sigma} \quad (22)$$

with the equivalent plastic strain rate, $\overline{\dot{\varepsilon}}_p$, damage rate, \dot{D} , and H' denoting the conventional hardening rate obtained as a slope of the true stress-true plastic strain curve, whereas χ and γ are additional constants depending on material and temperature. In this way, failure criteria and effect of damage on deformation before the failure are treated separately in the present approach.

APPLICATION OF THE CURRENT APPROACH

Outline of Experiments

Four materials were chosen as main materials targeted in this study. They include one austenitic stainless steel (SUS316 in Japan Industrial Standard), two ferritic steels (SQV2A

equivalent to A533B class 1 and SN400C) and one Nickel-base alloy (NCF 600), all of which are or planned to be in use in nuclear power plants.

Four kinds of specimens shown in Figure 1 were tested. They include conventional plain bar specimens, two kinds of circumferentially notched bar specimens with a notch of different geometries and grooved plate specimens. It should be pointed out that ω equals to 0 along the center line of plain bar and circumferential notched bar specimens due to axisymmetry whereas ω takes the value of approximately 1 due to the plain strain constraint in the grooved plate specimens. Difficulty of the treatment arises in the notched bar specimens where plastic strain near the notch root becomes larger than that at the center line of the specimen but at lower stress triaxiality and higher ω and the first failure may occur at different locations depending on material characteristics. Tests for all types of specimen were conducted at three temperatures ranging from room temperature (RT) to 300°C for ferritic steels and 400°C for others where creep effect is considered as insignificant. Displacement between two ridges or that measured by an extensometer of gauge length of 12.5 mm in the case of grooved plate specimens was controlled at the average strain rate of 0.1%/s.

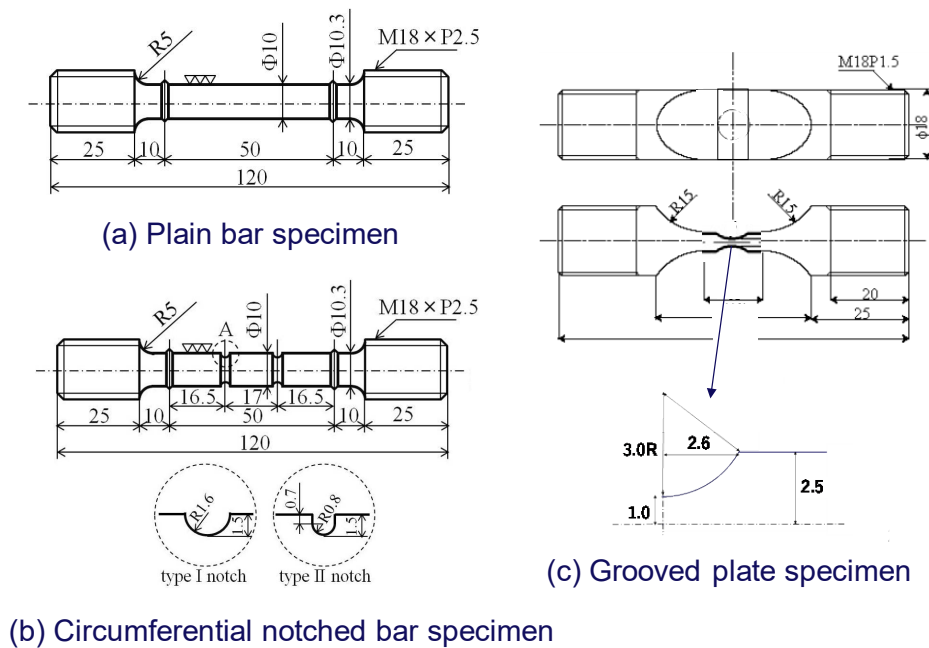


Figure 1 Geometry of test specimens (dimensions in mm)

Method of FE Analysis

General-purpose FE code, Marc ver, 2019, was used in this study. True strain-stress relations for each material and temperature were introduced by the user subroutine, “wkslp”. FE models used for each type of specimens are depicted in Figure 2. In the case of plain and notched bar specimens, 4-noded quadrilateral axisymmetric elements were used. Half of the specimen was analyzed due to symmetry in the case of plain bar specimen but a small imperfection of radius (-0.001mm) was given for 4 nodes near the symmetrical plane to make local necking occur around there intentionally. In the case of analyses for notched bar specimens, whole specimen was modeled but small difference in notch root radius was applied for two notches in order to simulate the situation where concentration of deformation and

subsequent fracture proceeds only in one notch after passing the maximum load. Finally, a quarter of grooved plate specimen was modeled by 8-noded three dimensional elements, in consideration of symmetry. In all analyses, large deformation formulation was activated and constant dilatation option was invoked as a default in MARC. Decrease of the flow stress according to eq.(22) was implemented by the user subroutine, “udamag” and elements were eliminated using deactivation option when the averaged damage variable within element reaches unity.

Material constants for each combination of material and temperature were determined through several trial and errors based on basic understandings on the role of each constant. Constants used in the final analyses are summarized in Table 1. It can be seen that most constants take the value covering a wide range depending on the material but also show some variation with temperature also.

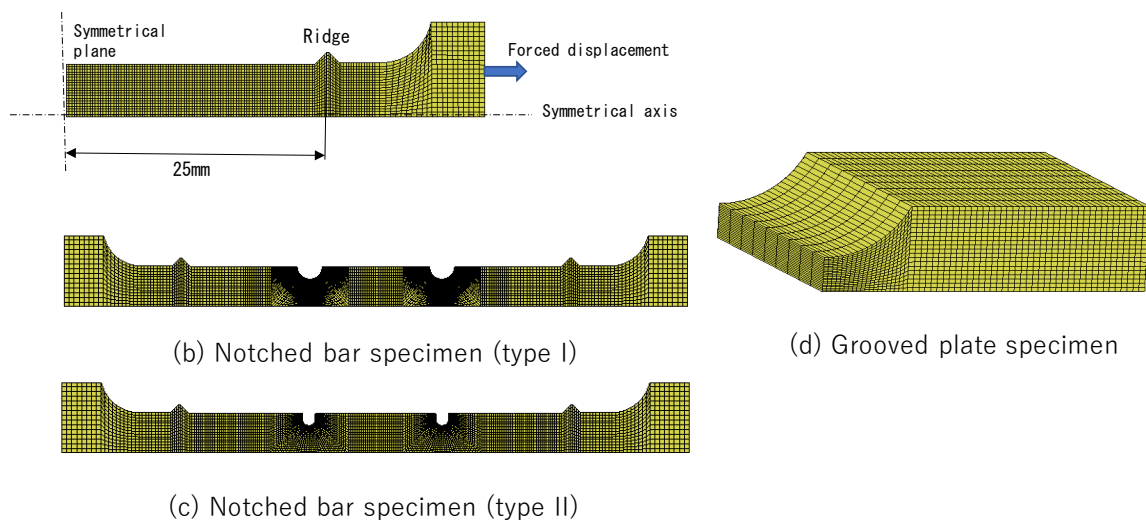


Figure 2 Mesh subdivision for each specimen

Table 1 Summary of material constants

Material	SQV2A(A533B)			SUS316 (316ss)			NCF600 (Alloy 600)			SN400C		
	RT	200°C	300°C	RT	200°C	400°C	RT	200°C	400°C	RT	200°C	300°C
ϵ_{f0}	3.0	3.9	3.0	2.8	2.7	1.8	1.7	2.3	1.2	3.2	1.8	3.2
α	0.50	0.75	0.55	0.40	0.40	0.40	0.50	0.63	0.63	0.50	0.50	0.55
ϵ_{fs}	1.00	0.93	0.66	1.40	2.50	1.50	0.55	0.50	0.62	3.20	1.80	3.00
β	0.10	0.10	0.10	0.18	0.40	0.19	0.03	0.06	0.06	0.50	0.50	0.55
γ	0.05	0.02	0	0	0	0.10	0.03	0.02	0.10	0	0	0
χ	0.31	0.21	0.11	0.08	0.25	0.43	0.03	0.09	0.05	0.16	0	0

Result of FE analysis

Figure 3 summarizes the results of analysis for the plain bar specimens in comparison with the experimental results on nominal stress – nominal strain relations. Here quick drops of the nominal stress is predicted due to the introduction of failure criterion into the analysis, in contrast to the previous analyses without it showing continues decrease with nominal strain. It can be seen that the results of analysis are in reasonably good agreement with the experimental data including the point of failure.

Then comparisons are made for load-displacement relations in notched bar and grooved plate specimens as shown in Figures 4 to 7. Reasonable agreement is attained between the test data and predictions obtained using the present equations at all temperatures for four materials. It might be useful to add that the deformation at failure of type I notch and type II notch specimens ranking differently depending on the material is reproduced by the analyses with a reasonable accuracy.

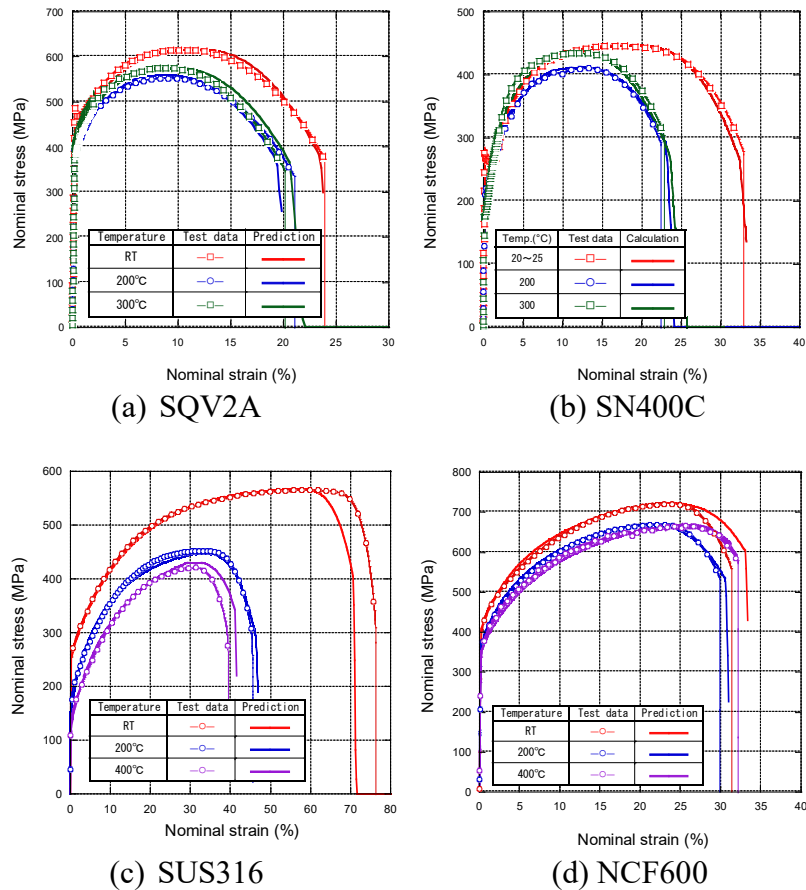


Figure 3 Comparison of nominal stress-strain relations in plain bar specimens

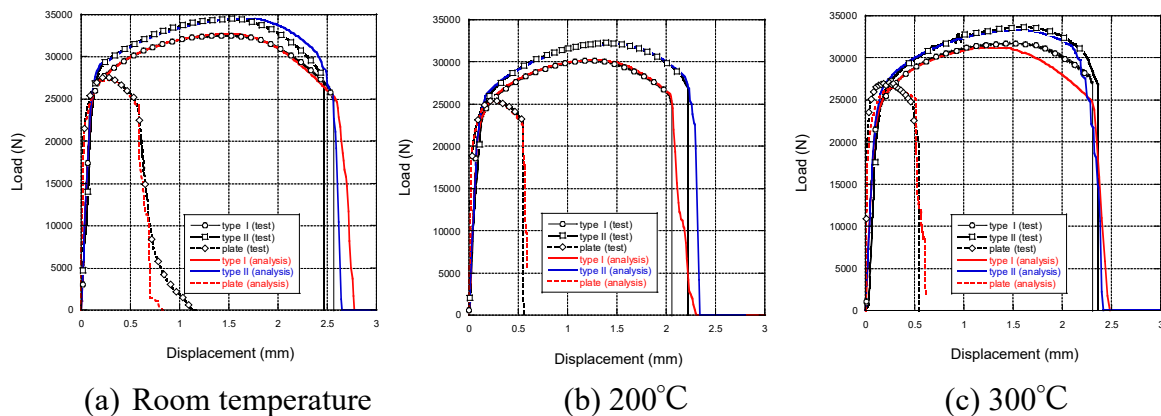


Figure 4 Comparison of load-displacement curves of notched specimens (SQV2A)

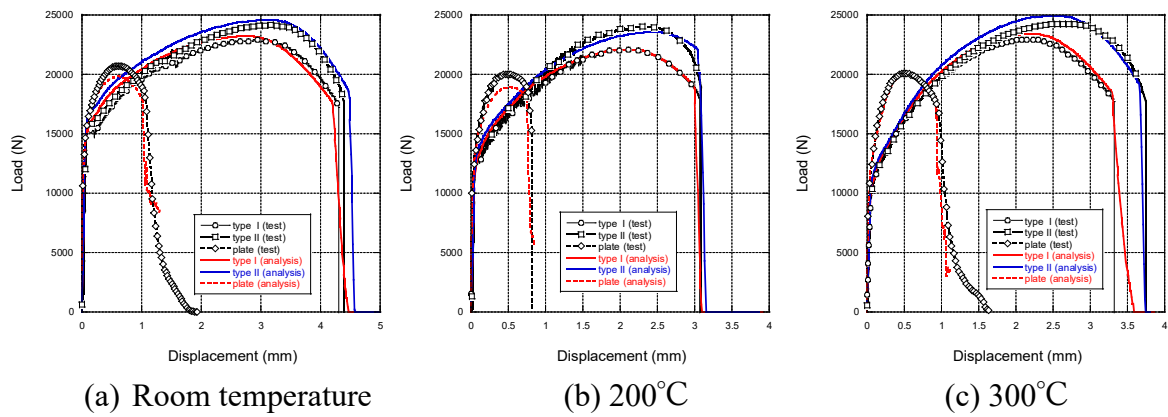


Figure 5 Comparison of load-displacement curves of notched specimens (SN400C)

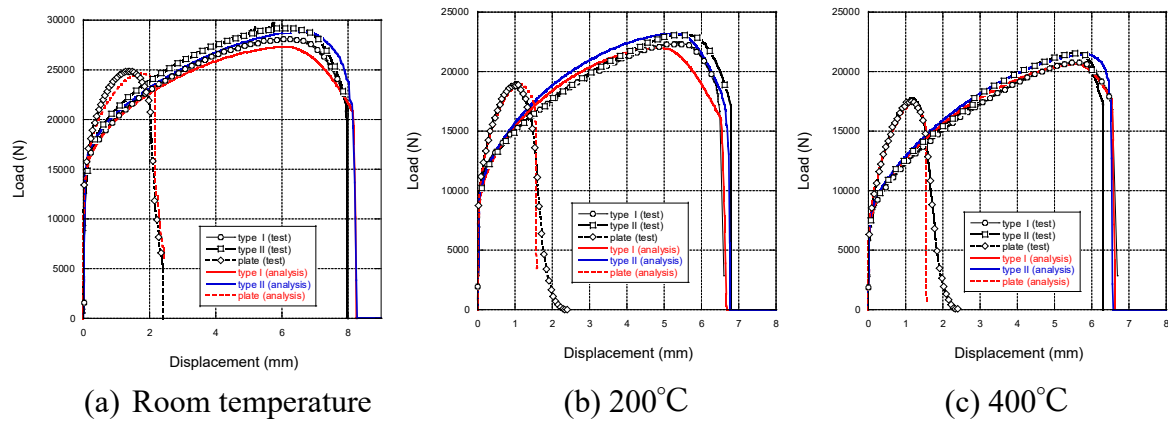


Figure 6 Comparison of load-displacement curves of notched specimens (SUS316)

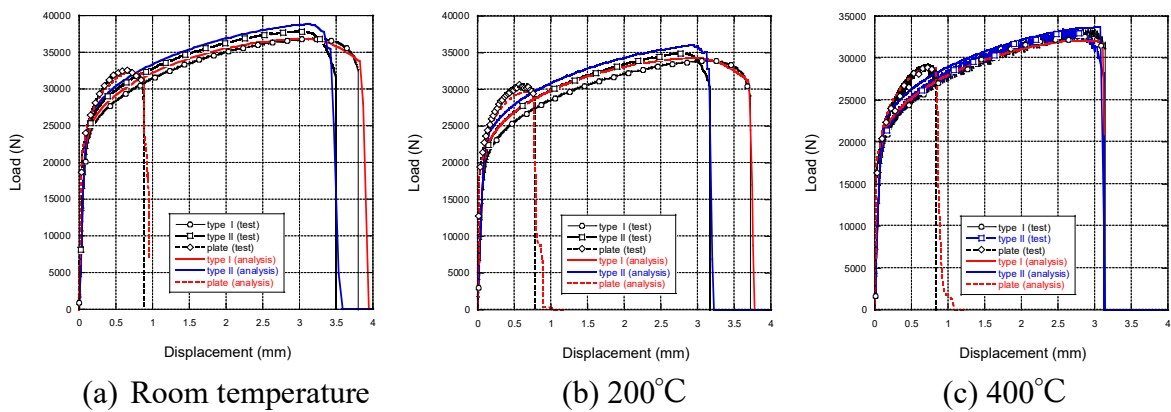


Figure 7 Comparison of load-displacement curves of notched specimens (NCF600)

CONCLUDING REMARKS

This paper presents the outline of the development of analytical tools for use in the prediction of local ductile fracture. This can be summarized as below:

- (i) Equations describing the relations between true stress and true plastic strain for a whole range of deformation in uniaxial tensile tests on plain bar specimens have been developed and shown to be reasonably accurate.
- (ii) A relatively simple approach was also developed for incorporating damage effect on deformation behavior and predicting local failure in consideration of the effect of stress triaxiality and the third invariant of deviatoric stress tensor. They were successfully applied to the evaluation of deformation and failure of various specimens including plain bar, two kinds of notched bar and grooved plate specimens, demonstrating the validity of the present approach.

REFERENCES

- American Society of Mechanical Engineers (2017), Boiler and Pressure Vessel Code, Section VIII, Division-2.
- Borona, N., Testa, G. (2022). "Plasticity damage self-consistent model incorporating stress triaxiality and shear controlled fracture mechanisms – model formulation," *Engineering Fracture Mechanics*, 271 108634.
- Gurson, A.L (1977). "Continuum theory of ductile rupture by void nucleation and growth: Part I - Yield criteria and flow rules for porous ductile media." *Trans. ASME, J Eng Mater Technol.*, 99(1) 2-15.
- Japan Society of Mechanical Engineers, (2014). "Structural integrity evaluation guideline under severe accident condition –BWR steel containment," JSME S NX2-2014 (in Japanese).
- Japan Society of Mechanical Engineers, (2015a). "Structural integrity evaluation guideline under severe accident condition –PWR prestressed concrete containment vessel," JSME S NX3-2015 (in Japanese).
- Japan Society of Mechanical Engineers, (2015b). "Structural integrity evaluation guideline under severe accident condition –PWR steel containment vessel," JSME S NX4-2015 (in Japanese).
- Japan Society of Mechanical Engineers, (2018). "Structural integrity evaluation guideline under severe accident condition –BWR reinforced concrete containment vessel," JSME S NX5-2018 (in Japanese).
- Oh, C.-S., Kim, N.-H., Kim, Y.-J., Baek, J.-H., Kim, Y.-P., Kim, W.-S., (2010). "A finite element ductile failure simulation method using stress-modified fracture strain model." *Engineering Fracture Mechanics*, 78(1) 124-137.
- Rice, J. R. and Tracey, D. M., (1969). "On the ductile enlargement of voids in triaxial stress fields," *Journal of Mechanics and Physics of Solids*, 17(3) 201-217.
- Takahashi, Y., (2018). "Trail for unified representation of monotonic stress-strain relations of various alloys," Proceedings of the ASME 2018 Pressure Vessels and Piping Conference.
- Takahashi, Y., (2021). "Development of stress-strain equations and local failure criteria for various alloys." The 13th International Conference on the Integrity of Nuclear Components.
- Takahashi, Y., (2023). "Progresses Towards the Guidelines for Evaluating the Strength Against Local Ductile Fracture," The 14th International Conference on the Integrity of Nuclear Components.
- Tvergaard V, Needleman A. (1984). "Analysis of the cup-cone fracture in a round tensile bar," *Acta Metall.*,32(1) 157–169.